Journal of Catalysis **204,** 428–439 (2001)
doi:10.1006/jcat.2001.3407, available online at http://www.idealibrary.com on IDEAL®

Nature of Active Sites in Sol–Gel TiO_2–SiO_2 Epoxidation Catalysts

C. Beck, T. Mallat, T. Bürgi, and A. Baiker[1]

Laboratory of Technical Chemistry, Swiss Federal Institute of Technology, ETH Hönggerberg, CH-8093 Zurich, Switzerland
E-mail: baiker@tech.chem.ethz.ch

Received May 16, 2001; revised August 31, 2001; accepted September 3, 2001

A series of titania–silica aerogels with 0–100 wt% TiO_2 content were synthesized and characterized by N_2 physisorption, DRIFT, UV-Vis, XPS, and ^{29}Si CP/MAS NMR analysis. It is shown that kinetic analysis of the epoxidation of 2-cyclohexene-1-ol (1) with TBHP is an informative test reaction providing insight in the nature of active sites. The surface area, pore volume, hydrophobicity, and relative abundance of Ti–O–Si linkages in the aerogels decreased with increasing Ti/Si ratio. Parallel to these changes, the initial rate of epoxide formation per Ti site (TOF) and the epoxide selectivity decreased but the productivity of the catalysts went through a maximum at 10 wt% TiO_2. We propose that due to kinetic effects in the sol–gel synthesis the whole range of active Ti sites may be present in the mixed oxides, spanning from tetrahedral Ti isolated by four SiO groups to octahedral Ti surrounded by six TiO groups in titania nanodomains. Ether formation from 1 was catalyzed by Brønsted sites present only on high titania-containing aerogels. Oligomerization was a major side reaction on all catalysts including Ti-free silica. Si-free titania was the most active in allylic oxidation of 1 to cyclohexenone. Silylation, or amine (Me_2BuN) addition to the reaction mixture, eliminated ether formation and suppressed oligomerization.

Key Words: **titania–silica; aerogel; cyclohexenol; epoxidation; TBHP; UV-Vis; FTIR; XPS; ^{29}Si CP/MAS NMR.**

1. INTRODUCTION

Titania–silica mixed oxides are active and selective epoxidation catalysts (1–11), offering an efficient alternative to the conventional titania-on-silica and Ti-substituted zeolites. The mixed oxides are usually synthesized by the sol–gel method and used in an organic medium with alkylhydroperoxides as oxidants. Despite the substantial effort in the past years, a comprehensive picture of the real nature of active sites in titania–silica could not be obtained. The main reason is the complexity of these materials: in contrast to the crystalline TS-1 (12, 13), numerous different structures are feasible in the amorphous aerogels and xerogels. These structures evolve during sol–gel synthesis, depending on the reactivity of precursors and on the conditions, and a remarkable restructuring may occur in the subsequent aging, drying, and calcination steps. A broad range of spectroscopic methods have been applied for structural characterization but the results are far less informative than in the case of well-defined, crystalline Ti-substituted zeolites. It is commonly accepted that, as an analogy to TS-1, good epoxidation activity and selectivity necessitates a high abundance of tetrahedral Ti sites, which are isolated by SiO "ligands" and act as Lewis acidic centers to activate the peroxide (8, 14, 15). Octahedral Ti in titania nanodomains diminish the catalytic performance.

It emerges from the mechanism of epoxidation that characterization of the acidity is crucial for understanding the nature of active sites. The mostly used characterization technique is the spectroscopic analysis of the adsorption of a volatile base on the dry solid (16–18). However, these results cannot really correlate with the catalytic performance in the liquid phase, where the peroxide, and possibly the solvent and reactant, coordinate to the active Ti site and change its acidity (19). For example, it has been demonstrated that the reactivity of titania–silica in the acid-catalyzed epoxide decomposition is strongly affected by the presence or absence of the peroxide (20, 21). A further complication is the formation of water during reaction by peroxide decomposition (22), as the addition of water generates new Brønsted sites (16) and thus may shift the product distribution.

To overcome these difficulties, we used the epoxidation of 2-cyclohexene-1-ol (**1**) as a test reaction for the *in situ* characterization of titania–silica. Beside epoxidation, the different acidic sites on titania–silica catalyze the ether (**3**) formation (dimerization) and oligomerization of reactant and products as shown in Scheme 1 (23). Additionally, allylic oxidation of **1** to cyclohexenone (**4**) and its slow further oxidation to epoxyketone (**5**) may also be important under the usual reaction conditions. Note that the epoxyketone (**5**) forms also on Ti-free silica in amounts comparable to that of the epoxide (**2**) (24).

UV-Vis diffuse reflectance, DRIFT, ^{29}Si CP/MAS NMR, and X-ray photoelectron spectroscopy completed the structural analysis of a series of amorphous mesoporous titania–silica aerogels covering a broad concentration range. Silylation and selective poisoning by addition of a soluble amine

[1] To whom correspondence should be addressed.

0021-9517/01 $35.00

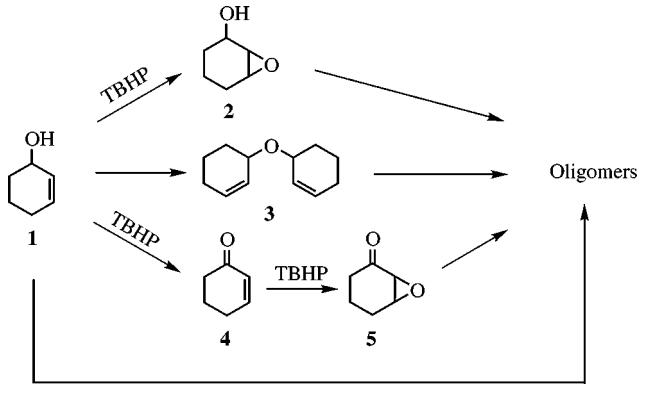

SCHEME 1. Major products formed in the epoxidation of **1** with titania–silica aerogels and TBHP.

to the reaction mixture are known strategies to improve the selectivity of titania–silica (25–29). Both techniques have been involved in the present study aiming at refining our knowledge on the structure–activity–selectivity relationship in titania–silica catalyzed epoxidation reactions.

2. EXPERIMENTAL

2.1. Materials

Analytical grade reagents and ion-exchanged water were used for the preparations. The abbreviation of aerogels is Ae-*X*, and Ae-*X-sil* after silylation, where *X* represents the fraction of TiO_2 content in weight percentage.

Amorphous mesoporous silica and titania–silica low-temperature aerogels (Ae-*X*) were prepared on the basis of a former recipe (10). The Si/Ti molar ratio were 1/0, 132/1, 54/1, 12/1, 5.3/1, corresponding to 0, 1, 2.5, 10, and 20 wt% TiO_2 for a theoretical catalyst TiO_2–SiO_2. A solution consisting of titanium–bisacetylacetonatediisopropoxide (Aldrich, 75 wt% in *i*-PrOH), tetramethoxysilane (Fluka, 99%), and 2.5 ml *i*-PrOH was prepared (for 2.5 g mixed oxide). The hydrolysant, consisting of 0.36 g HNO_3 (65 wt%), 3.26 g H_2O, and 10 ml *i*-PrOH, was added under vigorous stirring at room temperature. After 6 h, 1.54 g trihexylamine in 20.5 ml *i*-PrOH was added to the mixture. Gelation occurred within 0.2–24 h and the gel was aged for 6 days. Pure silica aerogels were prepared similarly without adding the Ti precursor.

TiO_2 aerogel (Ae-100) was prepared according to a former recipe (30). A solution of 31 mmol HNO_3, 120 mmol H_2O, and 10 ml MeOH was added to a solution of 40 ml MeOH and 31.2 mmol titanium-*n*-butoxide under vigorous stirring. Gelation occured after 1 min.

All above procedures were carried out in a glass reactor at room temperature under Ar. The resulting gel was semicontinously extracted with supercritical CO_2 in an autoclave, equipped with a glass liner. The extraction was completed within 5 h at 313 K and 200 bar with a CO_2 flow of 15 g min^{-1}. Portions of the raw aerogels were ground and heated in a tubular reactor in an upward air flow, at a rate of 5 K min^{-1} up to 673 K and kept at this temperature for 4 h. The samples were stored in air in a closed vessel and redried *in situ* before use.

Silylation of the calcined aerogel was carried out with *N*-methyl-*N*-(trimethylsilyl) trifluoracetamide (MSTFA, (31)): A solution of 0.6 g MSTFA (Aldrich, 99%) in 6 g toluene was added to the *in situ* redried (1 h, 473 K, Ar flow) aerogel sample (0.3 g). The slurry was stirred at room temperature for 2 h, then the catalyst was filtered, washed with toluene, and dried in air to give sample Ae-*X-sil*.

TS-1 (titanium silicalite, 3.1 wt% TiO_2, Si/Ti = 41/1) was prepared according to a known method (32).

2.2. Physico-Chemical Characterization

The specific surface area (S_{BET}), mean pore diameter ($\langle d_p \rangle$), and desorption pore volume $V_p(N_2)$ were evaluated by the BJH method and determined by nitrogen physisorption at 77 K using a Micromeritics ASAP 2000 instrument. Before measurement, the sample was degassed at 373 K until a final pressure below 0.1 Pa was achieved.

^{29}Si CP/MAS NMR measurements were performed on Bruker AMX 400 instrument. For the deconvolution of the Q^2, Q^3, and Q^4 MAS signals, starting values of −92, −100, and −108 ppm, respectively, were chosen. Peak positions and width of the peaks were not fixed. The Gaussian function was chosen as a fitting function and the fit was optimized using the least-squares method.

UV-Vis DRS measurements were performed on a Perkin–Elmer Lambda 16 spectrometer, equipped with an integration sphere. A 22-mg catalyst was diluted with 88 mg $BaSO_4$ and calcined at 300°C for 2 h, then sealed and measured after cooling. The resulting spectra were normalized. To evaluate the band gap of dry TiO_2–SiO_2, $[F(R_\infty)^* h\nu]^2$ was plotted against $h\nu$, where $h\nu$ is the energy of the incident proton and $F(R_\infty)$ is the Kubelka–Munk function. The linear part of the curve was extrapolated to zero absorption (33).

Diffuse reflectance infrared Fourier transform spectroscopy (DRIFT) was carried out on a Perkin–Elmer series 2000 instrument. The samples were prepared by mixing 10 mg aerogel with 90 mg dry KBr, and predried *in situ* at 573 K for 1 h in an Ar flow before the measurement at 50°C. Five-hundred scans were accumulated at a spectral resolution of 4 cm^{-1}. The relative Ti dispersion was estimated using the formula

$$D^*_{(Si\text{–}O\text{–}Ti)} = [S_{(Si\text{–}O\text{–}Ti)}/S_{(Si\text{–}O\text{–}Si)}][x_{Si}/x_{Ti}], \qquad [1]$$

where $S_{(Si\text{–}O\text{–}Ti)}$ is the deconvoluted peak area at approximately 935 cm^{-1} and $S_{(Si\text{–}O\text{–}Si)}$ the sum of the deconvoluted areas at approximately 1180 and 1228 cm^{-1}; x_{Si} and x_{Ti} designate the molar proportions of Si and Ti, respectively. The

following initial peak positions have been applied for deconvolution: 739, 792, 832, 930, 980, 1025, 1080, 1180, 1228 (+1260 for the silylated aerogels) cm^{-1}.

The X-ray photoelectron spectra were obtained using a Leybold LHS 11 instrument. MgK_α radiation (240 W) was applied to excite photoelectrons, which were detected with the analyzer operated at 38 eV constant pass energy. Sample charging was compensated using the C1s peak at 285.0 eV as internal standard. No significant differential charging of the samples could be observed.

2.3. Epoxidation Procedure

The epoxidation reactions were carried out batchwise in a mechanically stirred, 50-ml thermostated glass reactor equipped with thermometer, reflux condenser, and septum for withdrawing samples. All reactions were performed under Ar (99.99%). In a standard procedure, 100 mg aerogel was predried *in situ* in the reactor at 473 K for 1 h in an Ar flow. After cooling to room temperature, toluene (solvent), 0.5 ml dodecane (internal standard), and alternatively *N,N*-dimethylaminobutane (Aldrich, 99%, Ti/amine = 2.5 molar ratio) were added. The mixture was heated to 363 K, 10 mmol 2-cyclohexen-1-ol (Fluka, 97%) was added, and the reaction started by introducing 2.5 mmol *tert*-butylhydroperoxide (TBHP, Fluka, approx. 5.5 M in nonane, stored over molecular sieve 4A) to the vigorously stirred slurry. The total reaction volume was 10 ml.

The reaction mixture was analyzed using a HP 6890 gas chromatograph equipped with a cool on-column inlet and an HP-FFAP capillary column. Products were identified by GC-MS and by comparison with authentic samples. TBHP conversion was determined by iodometric titration using a Metrohm 686 Titroprocessor.

Initial (r_2) and average (r_{60}) reaction rates are characterized by the amount of epoxide formed in the first 2 and 60 min, respectively, and the values are related to unit time and catalyst surface area. Turnover frequency (TOF, mmol (**2**) s^{-1} mmol(Ti)$^{-1}$) indicates the amount of epoxide formed in the first 2 min, related to unit time and molar Ti content. The oxidation selectivities are calculated as follows:

Epoxide selectivity related to the olefin converted:

$$S_{\text{olefin}}(\%) = 100\{[\text{epoxide}]/([\text{olefin}]_o - [\text{olefin}])\}; \quad [2]$$

Epoxide selectivity related to the peroxide converted:

$$S_{\text{TBHP}}(\%) = 100\{[\text{epoxide}]/([\text{TBHP}]_o - [\text{TBHP}])\}; \quad [3]$$

where epoxide represents the epoxidation product of 2-cyclohexen-1-ol (**2**, Scheme 1), the subscript o stands for initial values, and all concentrations are expressed on a molar basis.

3. RESULTS

3.1. Catalyst Characterization

Nitrogen physisorption. N_2 physisorption measurements were carried out on calcined aerogels. All aerogels were mesoporous possessing an average pore diameter of at least 8 nm. Generally, increasing titania content and silylation of the aerogel diminished the BET surface area and pore volume (Table 1). Earlier studies revealed similar effects of silylation on the textural properties of TiO_2–SiO_2 (31, 34, 35).

NMR spectroscopy. The bulk structure of the aerogels before and after silylation was characterized by ^{29}Si CP/MAS NMR measurements (Table 1). As a measure of cross-linkage, the ratio of Q_4 to Q_3 sites are compared, with higher ratios indicating stronger cross-linking. Q denominates the presence of the corresponding Si sites in the spectra: $Q_4 = Si(OSi)_4$, $Q_3 = SiOH(OSi)_3$, and $Q_2 = Si(OH)_2(OSi)_2$. Silylation led to a strong enhancement of Q_4/Q_3 ratios due to replacement of the polar and hydrophylic SiOH groups by $SiOSi(CH_3)_3$ fragments. Unfortunately, the replacement was not complete, possibly due to a partial condensation of Q_3 to Q_4 sites during catalyst predrying at 423 K before silylation and a reversal of this process after silylation under ambient conditions.

Note that silylation is a proven strategy for reducing the hydrophilicity and improving the catalytic performance of TiO_2–SiO_2 and other Ti- and Si-containing epoxidation catalysts (31, 34–36).

TABLE 1

Structural Analysis by N_2 Physisorption, ^{29}Si CP/MAS NMR, and DRIFT Spectroscopies

Catalyst	S_{BET} ($m^2\,g^{-1}$)	$V_{p(N2)}$[a] ($cm^3\,g^{-1}$)	^{29}Si CP/MAS NMR Q^4 (%)	Q^3 (%)	Q^2 (%)	Q^4/Q^3	D*[b]
Nonsilylated aerogels							
Ae-0	1102	3.77	33.2	51.2	15.6	0.65	—
Ae-1	1056	3.06	34.9	53.8	11.3	0.65	26
Ae-2.5	936	3.01	—	—	—	—	—
Ae-10	976	2.77	41.1	44.0	14.6	0.93	4.4
Ae-20	761	1.46	—	—	—	—	—
Ae-100	248	1.21	—	—	—	—	—
Silylated aerogels							
Ae-0-sil	703	2.76	45.5	46.1	8.4	0.99	
Ae-1-sil	753	2.71	57.2	33.7	9.1	1.70	27
Ae-2.5-sil	675	2.75	—	—	—	—	—
Ae-10-sil	553	2.02	50.8	45.8	3.4	1.11	2.9
Ae-20-sil	421	1.16	—	—	—	—	—
Ae-100-sil	211	1.19	—	—	—	—	—

[a] Designates the BJH cumulative desorption pore volume of pores in the maximum range 1.7–300 nm diameter.

[b] Relative Ti dispersion determined by DRIFT spectroscopy; for definition see Experimental.

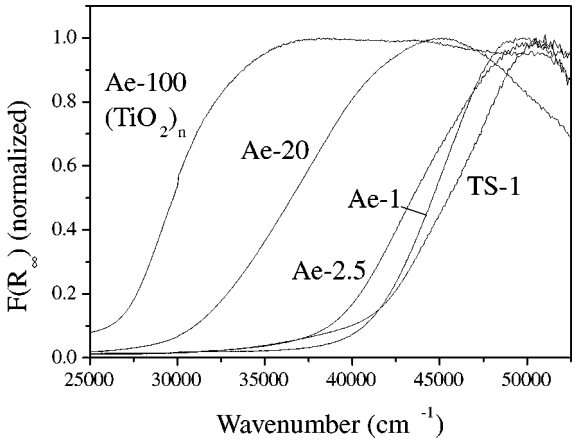

FIG. 1. Normalized UV-Vis spectra of titania–silica aerogels and TS-1.

UV-Vis DRS. UV-Vis spectroscopy has been commonly used to investigate the band structure of TiO_2–SiO_2 mixed oxides. At low Ti contents, blue shifts of band gap absorption edges occur, which originates from the quantum size effect, interface interaction (matrix support effect), and changes in coordination and ligand environment and the interatomic distances of TiO_2 microdomains (8, 37–42). Octahedral Ti sites are located at wavenumbers lower than those of tetrahedral sites and have lower band gap energies. LMCT (ligand-to-metal charge transfer) transitions can be estimated from the optical electronegativities of the ligand. For TS-1 the calculated transition peak at 48,000 cm^{-1} was confirmed experimentally. Therefore, Ti was assumed to exist in tetrahedral coordination in TS-1 (41), and later this crystalline material has served as a model for tetrahedral, isolated Ti sites in a silica matrix (43–45).

Hence, we also used TS-1 as a reference for the normalized spectra of the dehydrated aerogels (Fig. 1). To help evaluation of the band gap energies, the values extrapolated to zero absorption are plotted in Fig. 2 as a function of TiO_2 content. Since the samples were dehydrated, the contribution of OH groups and H_2O as ligands of Ti was minimized. As can be seen in Figs. 1 and 2, with decreasing Ti content in the aerogels the site isolation of Ti increases and approaches the "limit" value of TS-1. Still, there exists a small but significant difference between the LMCT band of TS-1 and the low titania content aerogels, in agreement with some earlier observations (4, 17, 42). This difference relative to TS-1 excludes complete site isolation in the low-titania-content aerogels.

DRIFT Measurements—Hydrophilicity of the aerogels. The aerogels containing 0, 1, and 10 wt% TiO_2 have been chosen for the IR study. The effects of silylation and *in situ* dehydration at 573 K in Ar are shown in Fig. 3 on the example of Ae-1. A comparison of curves a and b in the range 3000–3600 cm^{-1} confirms the removal of a considerable amount of adsorbed water during drying at 573 K. The bands in this range correspond to different stretching vibrations of hydroxyl groups (46), including the effect of absorbed water (3350 cm^{-1}) and the stretching vibrations of Si–OH groups (3590 cm^{-1}). The single peak at 3740 cm^{-1} is associated with isolated surface hydroxyl groups, typical for highly hydrophilic samples (47).

Silylation (Fig. 3, curves c and d) diminished the hydrophylicity of the aerogel, still, Ae-1-sil adsorbed a considerable amount of water under ambient conditions, as expected on the basis of earlier reports (25, 31). The new peaks in the spectrum of Ae-1-sil are assigned to C–H oscillation of the methyl group at 2960 cm^{-1}, the typical band of the Si–Me_3 group at 1260 cm^{-1}, and CH_3 rocking and Si–C stretching vibrations at 870–750 cm^{-1} (31). The presence of these bands indicates that the Si–OH groups have been extensively protected by Si–Me_3 groups.

Considering the spectra of all six aerogels we can conclude that hydrophylicity, reflected by the amount of adsorbed water, became more prominent with increasing

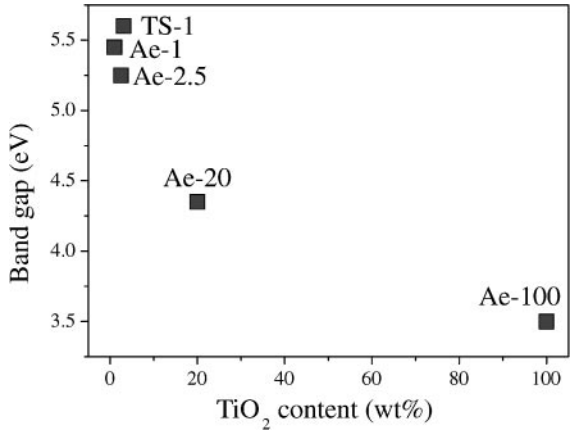

FIG. 2. Band gap energies of titania–silica aerogels and TS-1 determined from the UV-Vis spectra.

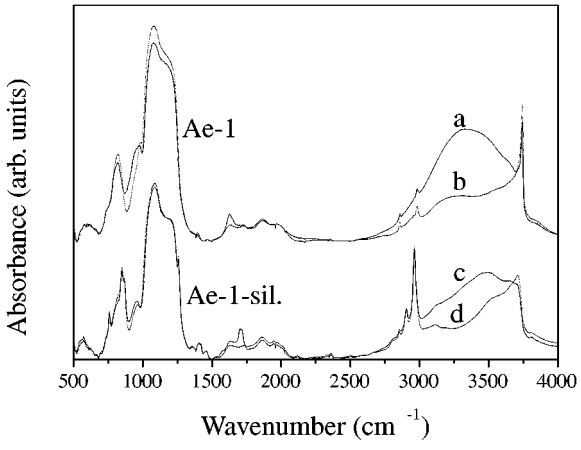

FIG. 3. Influence of predrying and silylation on the DRIFT spectrum of Ae-1 : Ae-1 (a) under ambient conditions and (b) after predrying at 573 K; and Ae-1-sil (c) under ambient conditions and (d) after predrying at 573 K.

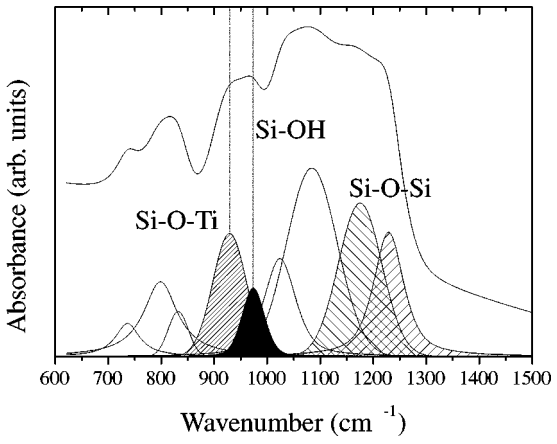

FIG. 4. Deconvolution of the DRIFT spectrum of Ae-10 to illustrate the determination of the relative Ti dispersion D^*; for definition see Experimental.

Ti content in both series of silylated and unsilylated samples.

DRIFT measurements—Ti dispersion. The IR band at 910–960 cm^{-1} is commonly accepted as the characteristic vibration of Ti–O–Si bonds in Ti- and Si-containing catalysts (19, 37). It was proposed that a comparison of the deconvoluted areas of this peak and the Si–O–Si peak at 1210 cm^{-1} provides a semi-quantitative estimate of the relative dispersion of Ti in the silica matrix (48, 49). This analysis may be disturbed by the vibration of Si–OH groups at around 980 cm^{-1} (50, 51), the additional contribution of Si bound to nonbridging oxygen (Si–O^-), and the effect of peak broadening by interaction of Si–OH or Si–O^- groups with adsorbed water (52, 53).

Here we tried to improve the semi-quantitative determination of Ti dispersion. Nine overlapping peaks (10 after silylation) in the range 600 and 1400 cm^{-1} were chosen for deconvolution into Gaussian curves (Fig. 4). The band assignments (31, 53, 54) and the positions after deconvolution are as follows: symmetric stretching vibrations of Si–O–Si bonds at 739, 792, and 832 cm^{-1}; the typical band of Si–O–Ti connectivity at 930 cm^{-1} and vibrations of Si–OH bonds at 980 cm^{-1}, both deconvoluted from the broad 960 cm^{-1} band; asymmetric Si–O–Si vibrations at approximately 1080, 1180 and 1228 cm^{-1}; Si–Me_3 fragments at 1260 cm^{-1}.

A comparison of the spectra of Ae-0, Ae-1, and Ae-10 samples revealed a strong overlapping of the Si–OH (980 cm^{-1}) and Si–O–Ti (~930 cm^{-1}) vibrations, resulting in the peak at around 960 cm^{-1}. Drying the aerogels at 573 K narrowed the Si–OH peak due to diminished interaction with adsorbed water, and silylation reduced the intensity of the peak. It seems to be important to silylate and/or carefully predry the aerogel at elevated temperature to improve the accuracy of peak deconvolution.

For determination of the refined relative Ti dispersion (D^*, Table 1) we compared the deconvoluted peak areas of the Ti–O–Si band at 930 cm^{-1} and the sum of the Si–O–Si bands at 1180 and 1228 cm^{-1} (yielding the peak at 1220 cm^{-1}). The standard deviation of the calculated values is estimated to be relatively high. Still, the remarkable difference between the relative Ti dispersions of the aerogels containing 1 and 10 wt% TiO_2 is impressive.

The Ti dispersions have been calculated also with the original formula, i.e., not excluding Si–OH vibrations (D, (49)). The differences between D and D^* were in the range 15–30%, relatively small compared to the differences caused by changes in the titania content (Fig. 5). Moreover, the D value for Ae-10 is very similar to that reported earlier for LT-10 (49). The Ti/Si ratio was the same for both aerogels. The main difference between the two series of aerogels is that here we applied a two-stage synthesis using a base catalyst in the second stage to facilitate condensation. The similar Ti dispersions in the aerogels containing 10 wt% titania indicate that the crucial step that determines the Ti dispersion in the silica matrix is the first, acid-catalyzed hydrolysis of the Ti and Si precursors.

The combined Ti dispersions of the two catalyst series show a hyperbolic decay with increasing titania content (Fig. 5). Thus, the DRIFT measurements corroborate the conclusion from the UV-Vis analysis (Fig. 2) that Ti site isolation decreases considerably with increasing TiO_2 content in the aerogels. A disadvantage of the DRIFT analysis is that the D and D^* values offer only a relative comparison and the absolute degree of site isolation cannot be judged.

X-Ray photoelectron spectroscopy. XPS analysis of titania–silica mixed oxides frequently indicate a linear relationship between surface and bulk composition below about 15 wt% TiO_2, and some surface enrichment in Si,

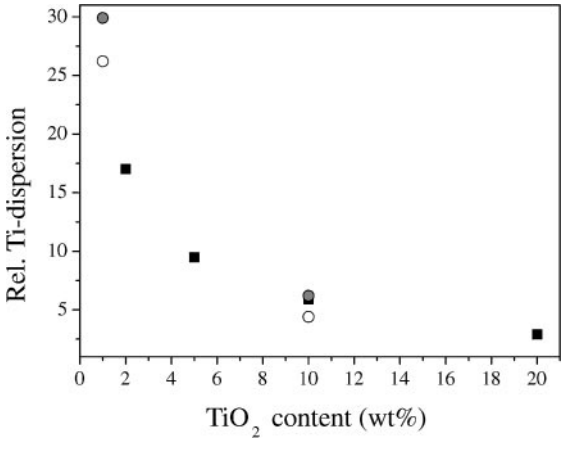

FIG. 5. Relative Ti dispersions D (including SiOH vibrations) and D^* (excluding SiOH vibrations), both estimated from the FTIR spectra. D (present work), (○); D^* (present work), (●); D from Ref. (49), (■); for the difference between D and D^* see text.

TABLE 2

Comparison of Binding Energies (Ti $2p_{3/2}$), and Surface and Bulk Compositions of TiO_2–SiO_2 Aerogels and TS-1

Catalyst	Si/Ti bulk ratio (at/at)	Ti/(Ti + Si) bulk (at%)	Ti/(Ti + Si) by XPS (at%)	BE (ΔBE[a]) (eV)
TS-1	41.6 : 1	2.35	2.4	460.3 (1.8)
Ae-1	132 : 1	0.75	0.8	459.9 (1.4)
Ae-2.5	54 : 1	1.82	1.7	460.0 (1.5)
Ae-10	12 : 1	7.7	5.9	459.9 (1.4)
Ae-20	5.3 : 1	15.9	13.7	459.1 (0.6)

[a] ΔBE (in parentheses) corresponds to the increase of the binding energy (BE) with respect to TiO_2 (BE: 458.5 eV).

particularly at high Ti content (37, 55, 56). Our results corroborate the earlier observations, as shown in Table 2. Significant differences between bulk and surface Ti content were obtained only for Ae-10 and Ae-20. The surface Si enrichment is attributed to the different reactivities of Ti and Si precursors in hydrolysis and condensation reactions during the sol–gel synthesis. Apparently, the reactivity of Ti-alkoxide, even when stabilized with acetylacetone, is higher than that of the Si-alkoxide. The higher reactivity of Ti-containing species leads to the formation of Ti-rich cores in the early stage of synthesis and the subsequent development of a Si-rich "shell." This effect might be minimized by prehydrolysis of the Si precursor (18, 49, 50).

The binding energies (BE) of Ti $2p_{3/2}$ core level in the titania–silica aerogels and TS-1 are collected in Table 2 and the corresponding spectra are shown in Fig. 6. The BE of the Ti $2p_{3/2}$ electron shifts with the coordination environment from about 458.5 eV for Ti in octahedral coordination (TiO_2, (57)) to about 460 eV for Ti in tetrahedral coordination in the silica lattice (56). Here, the BE values were the same for Ae-1, Ae-2.5, and Ae-10 and only slightly lower than the highest value measured for TS-1. The BE in Ae-20 is considerably shifted toward the characteristic value of TiO_2. These results indicate a change in coordination from octahedral to tetrahedral with decreasing Ti content, but still a gap of approximately 0.35 eV between low titania-content aerogels and TS-1 is obvious. Lassaletta *et al.* (39) proposed that, in addition to the effect of coordination environment, the titania–silica interface is important for the BE in XPS measurements. At the Ti–O–Si interface, the oxygen is less polarizable than bulk titania and the photoelectrons created at the titania–silica interface are less effciently screened than bulk titania.

Thus, assuming isolated tetrahedral Ti sites in TS-1, the BE values in the aerogels lower than those in TS-1 reveal an incomplete Ti-site isolation in the aerogels and the existence of TiO_2-clusters at high Ti content.

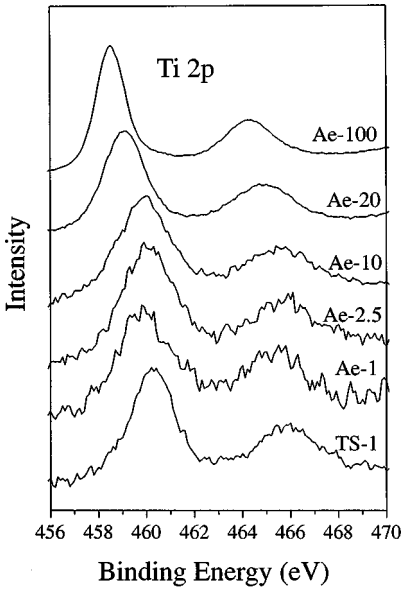

FIG. 6. XPS spectra of Ti 2p core levels of titania–silica aerogels and TS-1.

3.2. Catalytic Studies

General features of cyclohexenol epoxidation. The catalytic performance of all aerogels, before and after silylation and in the presence or absence of *N,N*-dimethylbutylamine additive, has been tested in the epoxidation of 2-cyclohexen-1-ol (**1**, Scheme 1) with TBHP as oxidant. The reactions were followed for 4–6 h, as illustrated by the example of Ae-1 in Fig. 7. At low conversion the epoxidation was fast and selective: 50% conversion was achieved in 7.5 min and the selectivity to epoxide related to the olefin (S_{olefin}) and peroxide (S_{TBHP}) were 81.5 and 85%, respectively. Note that the molar ratio **1**/TBHP was 4/1, and the conversion

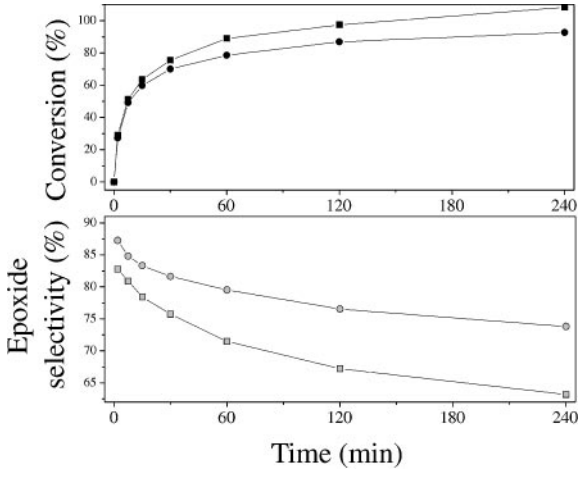

FIG. 7. Kinetic analysis of the epoxidation of 2-cyclohexen-1-ol with Ae-1 and TBHP under standard reaction conditions. (Top) Conversion of olefin (■) and TBHP (●); (bottom) epoxide selectivities related to olefin (□) and TBHP (○) consumed, S_{olefin} and S_{TBHP}, respectively.

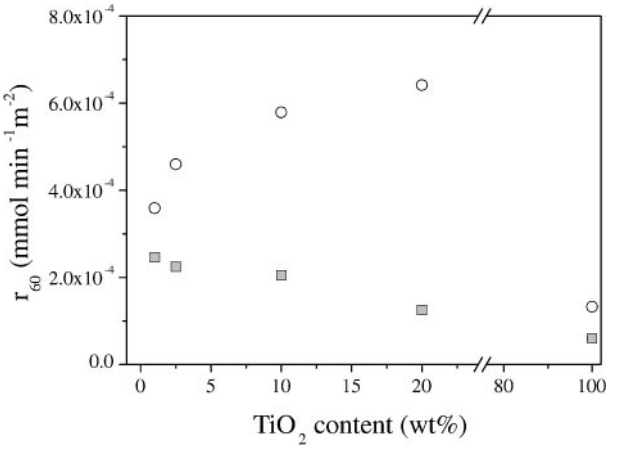

FIG. 8. Influence of TiO_2 content and silylation on the average reaction rate characterized by the epoxide formation in 60 min (r_{60}); standard reaction conditions. ◯, silylated, and ▢, unsilylated.

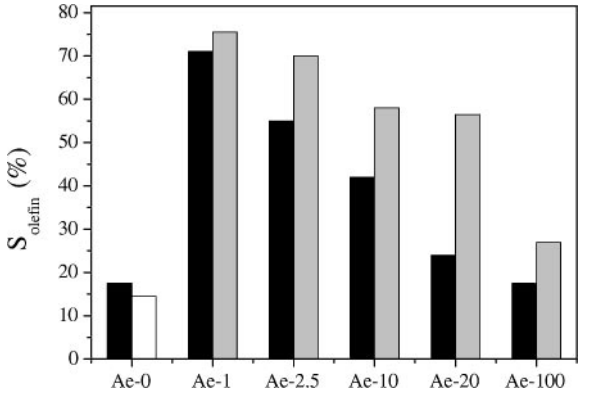

FIG. 9. Influence of TiO_2 content before (black bars) and after silylation (gray bars) on the epoxide selectivity related to the olefin converted in 60 min (S_{olefin}); standard reaction conditions.

was related to the limiting reactant TBHP. The epoxide selectivities dropped with increasing conversion (Fig. 7, bottom). This effect is attributed mainly but not exclusively to the side reactions presented in *S*cheme 1. We have shown recently (24) that oxidation with Ti-free silica and also the uncatalyzed (background) oxidation are slow but after long reaction times their contribution is significant. These reactions afford mostly allylic oxidation products and oligomers, and thus limit the epoxidation selectivity of titania–silica mixed oxides to a certain degree.

The activity of aerogels, characterized by the epoxide formation in the first 60 min (r_{60}), decreased monotonously with increasing titania content (Fig. 8). Silylation enhanced the epoxidation rate in all cases and the higher the titania content, the higher was the positive influence of silylation (up to 200 rel.% in the case of Ae-20). In contrast, amine addition always decreased the rate, although the difference was negligible for Ae-20 (not shown). It has been reported earlier (23, 27, 58) that also the chemical structure of the amine and the Ti/amine ratio influenced the epoxidation rate and selectivity. For the sake of clarity, here only *N,N*-Dimethylbutylamine was used and the Ti/amine molar ratio was kept constant at 2.5. Figure 8 shows that the epoxidation activity of titania (Ae-100) is small but not negligible. This confirms our earlier proposal that titania nanodomains in titania–silica mixed oxides should be considered as moderately active and selective epoxidation sites (2).

Silylation improved the selectivity of all Ti-containing aerogels (Fig. 9). The highest influence of silylation and amine additive on the epoxide selectivity was observed with Ae-20 (Fig. 10). As the selectivity strongly varied with conversion, both S_{TBHP} and S_{olefin} values were compared at 50% conversion of the peroxide and olefin, respectively. Silylation was clearly more efficient than amine addition, affording up to 80% peroxide selectivity. The amine modifier had even a negative impact on the selectivities when added to the silylated sample Ae-20-sil. A probable reason is the dealkylation of the tertiary amine to imine by TBHP (59).

For comparison, a 20 wt% titania–80 wt% silica aerogel hydrophobized by methyl groups covalently bound to the silica matrix afforded 90% conversion of **1** in only 10 min reaction time, and the epoxide selectivity was 98% (28). On the other hand, modification of a 20 wt% titania–80 wt% silica aerogel by soluble amine additives improved the selectivity in the same reaction only up to 81% and the reaction rate was always lower in the presence of the amine (23). These data confirm that hydrophobization is a more efficient strategy for improving the performance of titania–silica mixed oxides.

Characterization of the aerogels by the initial rate and selectivity. Kinetic analysis of the epoxidation of **1** over the aerogels with high titania content revealed a gradual loss of activity with time. Catalyst deactivation is mainly

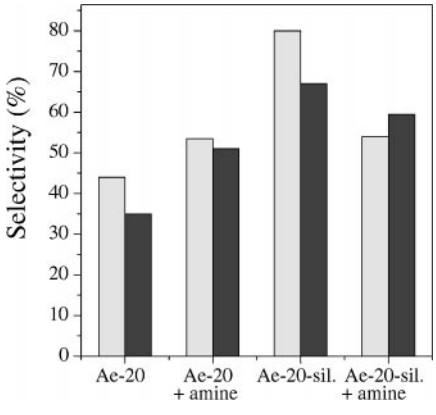

FIG. 10. Effect of silylation and amine additive on the epoxide selectivities of Ae-20. The selectivities are related to the peroxide (S_{TBHP}, gray bars) or olefin (S_{olefin}, black bars) consumed; standard reaction conditions.

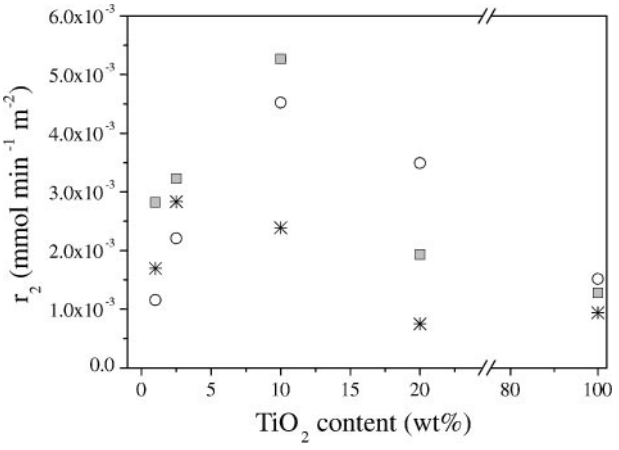

FIG. 11. Initial rate (r_2) of epoxide formation as a function of TiO_2 content and silylation; standard reaction conditions. ■, Ae-*X*; ○, Ae-*X*-*sil*; ✳, Ae-*X* + amine.

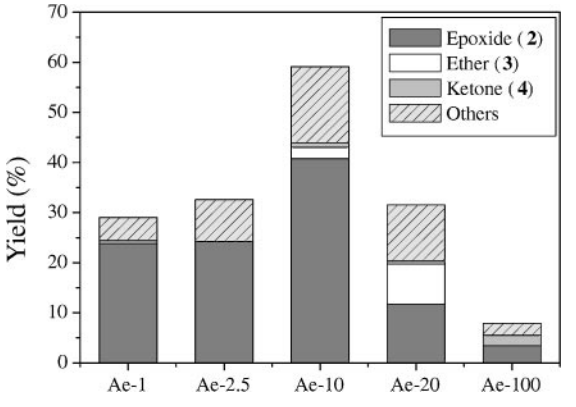

FIG. 13. The effect of titania content on the formation of epoxide (**2**), ether (**3**), ketone (**4**), and other products (mainly oligomers); 2 min reaction time, standard conditions.

attributed to oligomer formation and blocking of a fraction of active sites. In order to minimize this effect, the structure–activity–selectivity relationship was investigated further by considering the initial performance of the aerogels on the basis of samples taken after 2 min reaction time.

In Fig. 11 the initial rate of epoxide formation (r_2) is characterized by the amount of epoxide formed in 2 min and related to the unit surface area of the aerogel. There is a clear optimum at 10 wt% TiO_2 content, including both the silylated and unsilylated aerogels. (Note the remarkable differences compared to the r_{60} values in Fig. 8.) A completely different picture is obtained when the initial rate of epoxide formation is related to the titania content of the aerogel (Fig. 12): the TOF values diminished rapidly with increasing titania content. In fact, the TOF values are slightly distorted by the deviation between surface and bulk Ti content and by the activity of the silica matrix (24). The effect of silylation was always negative (low titania content) or negligible (high titania content). It has been proposed recently that the lower initial rate after silylation may be due to reduced accessibility of active sites caused by the bulky trimethylsilyl groups and possibly to a weaker adsorption of the allylic alcohol on the hydrophobic surface (34).

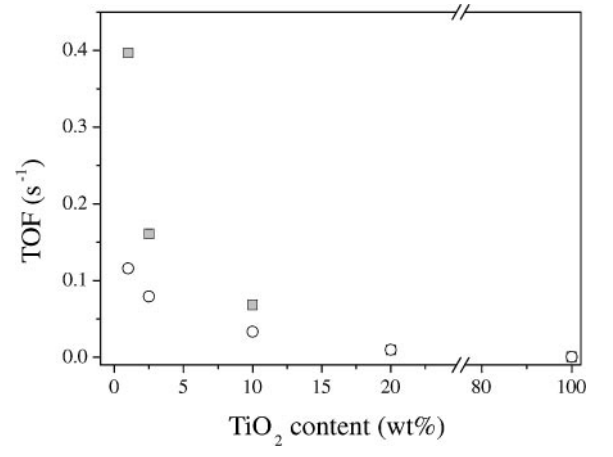

FIG. 12. Initial turnover frequencies (TOF) as a function of TiO_2 content before (■) and after silylation (○); standard reaction conditions.

N,N-Dimethylbutylamine always reduced the initial rate of epoxide formation, but the effect was more pronounced for the high titania content aerogels Ae-10 and Ae-20 (Fig. 11). A similar impact was observed when the amine was added to the silylated aerogels (not shown). Poisoning by the amine was small or even absent when reaction times of 60 min or longer were considered. Obviously, the amine additive diminishes the formation of some byproducts that are responsible for deactivation of the aerogels, particularly Ae-10 and Ae-20.

The influence of titania content on the product distribution after 2 min reaction time is depicted in Fig. 13. Interestingly, already after 2 min the dominant side reaction was the formation of dimers and oligomers from the reactant and products (shown as "others"). Ketone (**4**) and epoxyketone (**5**) together accounted for maximum 5% of the olefin converted, so oligomers and minor unidentified products build up the main part of "others." Ae-1 afforded the highest initial epoxide selectivity. Ether (**3**) formation was detectable only on the high titania-content aerogels Ae-10 and Ae-20. Allylic oxidation of **1** to cyclohexenone (**4**) was the fastest on titania (Ae-100), and it was not detectable with Ae-2.5. The other allylic oxidation product, the epoxyketone (**5**) formed only in small amounts, never exceeding 25% of cyclohexenone (**4**). As oxidation of the OH function of the epoxide cannot be excluded under the conditions applied, only the amount of **4** is used to characterize the extent of allylic oxidation of **1**.

Considering only the least selective mixed oxide Ae-20, the effects of amine additive and silylation are illustrated in Fig. 14. Both treatments eliminated ether (**3**) formation and reduced oligomerization, but none of them could suppress

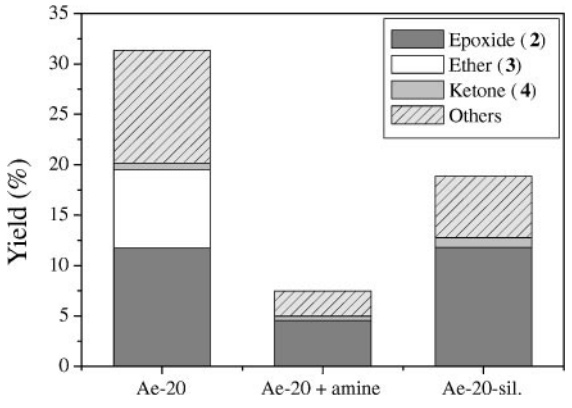

FIG. 14. Influence of amine addition and silylation on the formation of epoxide (**2**), ether (**3**), ketone (**4**), and other products (mainly oligomers); 2 min reaction time, Ae-20, standard conditions.

allylic oxidation to the corresponding ketone (**4**). *N,N*-Dimethylamine strongly diminished the conversion of **1** to any product.

4. DISCUSSION

4.1. Nature of Active Sites in Titania–Silica Mixed Oxides

It is commonly accepted that tetrahedral Ti isolated by SiO groups in the silica matrix is the most active site in titania–silica epoxidation catalysts, including silicalites and mixed oxides (12, 60–62). As shown schematically in Fig. 15a, this Lewis acidic site is responsible for activation (coordination) of the alkylhydroperoxide, and thus for the oxygen transfer to the olefin. A bidentate complex has also been proposed for epoxidations with TS-1 and H_2O_2 (Fig. 15b), but this structure is less likely in case of the bulky TBHP as oxidant. The polar solvent, the coproduct alcohol formed from the peroxide, the amine additive, and also the allylic alcohol as reactant can interact with Ti tripodally anchored to silica, leading to the stable octahedral coordination (15, 19, 27, 63, 64). Our results confirm that isolated tetrahedral Ti is the most active and selective site for olefin epoxidation. The abundance of these sites increases sharply with decreasing Ti/Si ratio in the aerogels as illustrated by

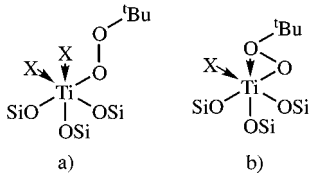

FIG. 15. Schematic representation of two possible structures (a, b) of isolated tetrahedral Ti, tripodally anchored to silica and coordinated by TBHP and some reaction components (X). X = O- or N-containing molecule.

the band gap energies derived from UV-Vis measurements (Fig. 2), the relative Ti dispersion calculated from DRIFT spectroscopy (Fig. 5), and the shift in binding energies of Ti $2p_{3/2}$ core level electrons determined by XPS (Fig. 6). Parallel to enhanced site isolation, the initial TOF in the epoxidation of **1** (Fig. 12) and the initial epoxide selectivity (Fig. 13) increased remarkably with decreasing TiO_2 content.

The other commonly accepted active species dominant at high Ti/Si ratios is the octahedral Ti in titania nanodomains. The shifts of the UV-Vis and XPS spectra of mixed oxides toward those of anatase titania are interpreted as evidence (among others (8, 37)) for the presence of titania nanodomains in the mixed oxides. Figures 12 and 13 demonstrate that the titania aerogel Ae-100, characterized by a few nanometers primary particle size (30), possesses poor selectivity (<15%), and its initial epoxidation activity expressed as TOF is ~900 times lower than that of Ae-1, the most active mixed oxide. This ratio is ~1600 : 1 when the average TOF values are compared after 1 h reaction time. In the epoxidation of cyclohexene the ratio between the average TOF of the most and least active aerogels 5 wt% TiO_2–95 wt% SiO_2 and TiO_2, respectively, was 350 (2). Titania is a Lewis acidic oxide (65), and its acid strength increases by several orders of magnitude with decreasing particle size (66).

The complex catalytic behavior observed in the epoxidation of **1** cannot sufficiently be interpreted by the assumption of only isolated tetrahedral Ti and TiO_2 nanodomains. Considering the high reactivity of various Ti- and Si-containing species in hydrolysis and condensation reactions during sol–gel synthesis, it is reasonable to assume that the final distribution of active sites is governed mainly by kinetic factors. Hence, several different Ti-containing species may be present in the mixed oxides. Their structure can cover the whole range from tetrahedral Ti isolated by four SiO groups to octahedral Ti surrrounded by six TiO groups (titania nanodomains) (67). The transformation of isolated, tetrahedral Ti to octahedral TiO_2 nanodomains may be visualized by a gradual replacement of SiO ligands by TiO groups, and a change from 4 to 5 to 6 coordination (Fig. 16a). The first "step" in this direction is the bidentate Ti site. This structural unit is present in the soluble titanosilsesquioxane prepared from $Ti(O^iPr)_4$ and trisilanols (Fig. 16b, (68)), and also in silica-supported $Ti(O^iPr)_4$ (Fig. 16c, (69)). Both catalysts are active and selective in the epoxidation of cyclohexene with TBHP. Hence, a complete site isolation in titania–silica cannot be a sufficient prerequisite to produce a good epoxidation catalyst. This conclusion contrasts with the structural requirements of crystalline Ti-substituted zeolites (19).

The last step in the "hypothetic" change from isolated Ti to anatase titania is a Ti site that contains only Ti–O–Ti connectivities except one Ti–O–Si bond (Fig. 16d). We assume that this structure formed when the surface OH

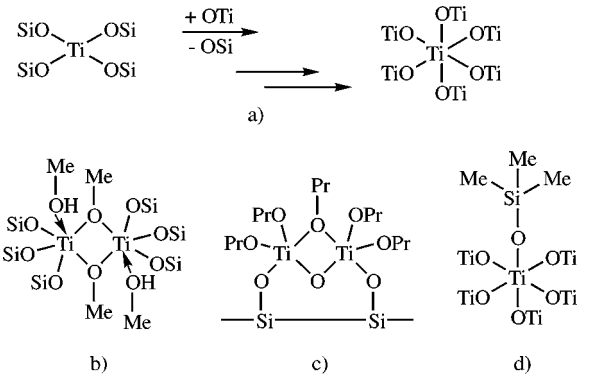

FIG. 16. Schematic representation of acitve sites in titania–silica mixed oxides covering the whole range from isolated tetrahedral Ti to octahedral Ti in anatase TiO_2 nanodomains (a); titanosilsesquioxane as epoxidation catalyst (68) (b); the proposed active site in silica-supported $Ti(O^iPr)_4$ (69) (c); and silylated octahedral titania (d).

groups of the titania aerogel were silylated (Ae-100-sil). The difference in initial activity between Ae-100 and Ae-100-sil was minor (r_2, Fig. 10) but after 4 h the epoxide yield increased from 4.2 to 8.3% and, despite the higher conversion, the selectivity (S_{olefin}) increased from 12.6 to 19.2%.

In fact, the schematic illustration of active sites in Fig. 16 is further complicated by the easy hydration of the Ti–O–Si bond, producing Ti–OH and Si–OH functions and leading to 4, 5, and 6 coordinated Ti(OH) (and $Ti(OH)_2$) species (64). DRIFT analysis (Fig. 3) indicated that calcination and silylation eliminated the Si–OH (and TiOH) groups only partially. Water formed from peroxide decomposition during epoxidation further enhances the abundance of these species. Our former study proved that application of zeolite 4A as a drying agent in the epoxidation of **1** significantly improved the selectivity of titania–silica (28). This observation is an indirect evidence for the lower efficiency of the "hydrated" Ti active sites but unambiguous identification of these sites is not yet possible.

4.2. Role of Surface Si–OH Groups

Ti-free silica, despite the presence of Si–OH functions, is not acidic (65). Nevertheless, these functional groups have been assumed to be the active sites for the acid-catalyzed solvolysis of some epoxides, and suppression of this side reaction after silylation of TS-1 supported the hypothesis (19). Here we also found a pronounced positive effect of silylation on the performance of titania–silica. During silylation the Si–OH and Ti–OH groups are (partly) transformed to Si–O–Si and Ti–O–Si connectivities. The change in rate and product distribution may be attributed to this chemistry but also to different hydrophobicities of the surface, resulting in changes in the adsorption of the reactant, and to lower accessibility of Ti sites due to the bulky trimethylsilyl groups. We have found recently (70) that the surface Si–OH groups are poor catalysts for epoxide decomposition when compared to the Lewis acidic Ti sites coordinated by the peroxide, but the latter sites catalyze epoxidation rather then epoxide decomposition until the olefin reactant is present.

To obtain a clear answer concerning the role of Si–OH groups as active sites, we compared the performance of Ae-0 and Ae-0-sil to the background oxidation (more details can be found in a former report (24)). Figure 17 presents the product distributions after 4 h reaction time; due to the low reaction rate the initial values could not reliably be determined. Obviously, Si–OH groups play an important role in acid-catalyzed oligomerization (major part of "others") and silylation efficiently suppresses this activity. A comparison of the yields with Ae-0-sil and without catalyst reveals that silylation completely eliminated the allylic oxidation of cyclohexenol to cyclohexenone (**4**). Hence, we can conclude that, similarly to TS-1 catalyzed epoxidations (19), the contribution of surface Si–OH groups in various side reactions cannot be neglected.

4.3. Brønsted Acidity at High Titania Content

Dimerization of cyclohexenol to the unsaturated ether **3** (Scheme 1) is catalyzed by Brønsted sites. This side reaction was significant only on titania–silica aerogels containing at least 10 wt% TiO_2 (Fig. 12). The amount of **3** increased with increasing TiO_2 content but the reaction was completely blocked by silylation or amine addition to the reaction mixture (Fig. 13).

There are different explanations for the nature of Brønsted acidic sites in titania–silica. According to a widely accepted model, Brønsted acidity is associated with the Ti–O–Si linkages where the Ti atoms are located in penta- or octahedral sites (16, 17, 37). The local charge imbalance is compensated by protons (71). Surface hydroxylation (hydration) is also important for generation of acidity. The

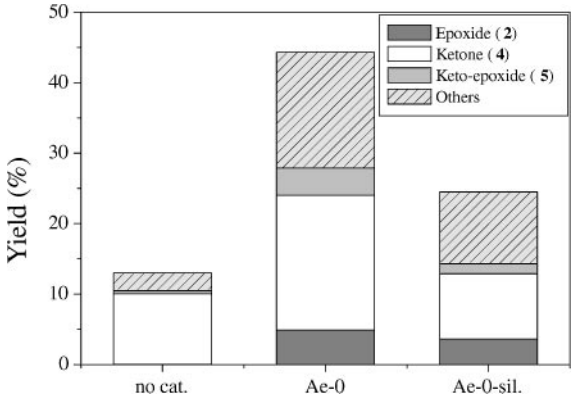

FIG. 17. Epoxidation of 2-cyclohexene-1-ol (**1**) without catalyst, and with Ae-0 and Ae-0-sil, leading to epoxide (**2**), cyclohexenone ("ketone," **4**), cyclohexenone-epoxide ("keto-epoxide"), and other products, mainly oligomers. Yields are measured after 4 h reaction time; standard conditions.

Si–OH group acts as an O-donor ligand for Ti, forming the bridging hydroxyl group Ti–O(H)–Si (72). Combination of these models can well explain our observations that: (i) significant Brønsted acidity developed only in aerogels that contained considerable amount of octahedral Ti (Ae-10 and Ae-20), (ii) the acidity (lower epoxidation selectivity) of mixed oxides increased upon hydration, and (iii) the formation of ether (**3**) after silylation was eliminated.

4.4. Role of Amine Additive

N,N-Dimethylbutylamine additive acts as a selective poison in the epoxidation of cyclohexenol. The initial reaction rate was always lower in the presence of amine (Fig. 11), the effect of which is attributed to coordination to the Ti sites leading to reduced acidity and reactivity (Fig. 15). This coordination enhanced the selectivity (S_{olefin}), particularly for aerogels with high Ti/Si ratio (Fig. 10). The amine additive efficiently suppressed the acid-catalyzed oligomerization and completely eliminated the ether (**3**) formation. Apparently, amines block the less selective sites stronger than the most active and selective sites, the isolated tetrahedral Ti. Addition of amine reduced the epoxide selectivity of Ae-1, as this aerogel contains dominantly isolated Ti sites.

An important observation is that silylation is more efficient in improving the selectivity of aerogels with high Ti/Si ratio than amine addition (Fig. 14). No positive effect was achieved when the amine was applied together with any of the silylated aerogels (see, e.g., Fig. 10). The addition of amine always decreased the rate of epoxide formation, although the effect was minor after 1 h reaction time. In contrast, silylation enhanced the average rate remarkably (Fig. 8). The difference between the effects on the initial and average rates is due to the formation of oligomers and blocking a fraction of active sites; these side reactions are suppressed to some extent by both treatments, amine addition or silylation.

5. CONCLUSIONS

Epoxidation of 2-cyclohexene-1-ol (**1**) is a good test reaction for complementing the spectroscopic characterization of titania–silica mixed oxides. The presence of two reactive functional groups in the molecule leads to a complex reaction network including acid-catalyzed epoxidation, ether formation, and oligomerization, as well as allylic oxidation reactions. Kinetic analysis of the rate of these reactions provides useful information on the nature and abundance of various active sites in titania–silica. The study of aerogels containing 0–100 wt% TiO_2 indicated the presence of various active Ti sites covering the whole range from tetrahedral Ti surrounded by only SiO ligands to octahedral Ti surrounded by TiO ligands in titania nanodomains. We propose that complete site isolation is not a necessary requirement for preparing active and selective titania–silica epoxidation catalysts. Mainly due to kinetic effects during the sol–gel synthesis, the lower the Ti/Si ratio, the higher is the relative abundance of isolated tetrahedral Ti sites in the aerogels and these catalysts exhibit the highest epoxidation activity and selectivity per Ti site (TOF). From a technical point of view the productivity, i.e., the rate of product formation related to the amount of catalyst, is important, and in this respect the 10 wt% TiO_2–90 wt% SiO_2 aerogel is the best choice. (A former study revealed an optimum in productivity at 20 wt% TiO_2 for cyclohexene epoxidation (2).)

Dimerization of cyclohexenol to an unsaturated ether is catalyzed by Brønsted sites developed only at a high Ti/Si ratio. Oligomerization is catalyzed by various acidic sites and even the silanol groups in the silica matrix play a role in this side reaction. The performance of aerogels can be improved by silylation of the carefully predried aerogel or by addition of a tertiary amine to the reaction mixture (selective poisoning of the acidic sites). The latter method is simpler but less efficient.

ACKNOWLEDGMENTS

The authors are grateful to D. Ferri for deconvolution of DRIFT spectra and to F. Bangerter for NMR measurements.

REFERENCES

1. Imamura, S., Nakai, T., Kanai, H., and Ito, T., *Catal. Lett.* **28**, 277 (1994).
2. Hutter, R., Mallat, T., and Baiker, A., *J. Catal.* **153**, 177 (1995).
3. Imamura, S., Nakai, T., Kanai, H., and Ito, T., *J. Chem. Soc.-Faraday Trans.* **91**, 1261 (1995).
4. Liu, Z., Crumbaugh, G. M., and Davis, R. J., *J. Catal.* **159**, 83 (1996).
5. On, D. T., Kapoor, M. P., and Kaliaguine, S., *Chem. Commun.* 1161 (1996).
6. Dutoit, D. C. M., Schneider, M., Hutter, R., and Baiker, A., *J. Catal.* **161**, 651 (1996).
7. Klein, S., Thorimbert, S., and Maier, W. F., *J. Catal.* **163**, 476 (1996).
8. Davis, R. J., and Liu, Z. F., *Chem. Mater.* **9**, 2311 (1997).
9. Dusi, M., Mallat, T., and Baiker, A., *J. Catal.* **173**, 423 (1998).
10. Müller, C. A., Gisler, A., Schneider, M., Mallat, T., and Baiker, A., *Catal. Lett.* **64**, 9 (2000).
11. Mallat, T., and Baiker, A., *Appl. Catal. A* **200**, 3 (2000).
12. Notari, B., *Catal. Today* **18**, 163 (1993).
13. Gleeson, D., Sankar, G., Catlow, C. R. A., Thomas, J. M., Spano, G., Bordiga, S., Zecchina, A., and Lamberti, C., *Phys. Chem. Chem. Phys.* **2**, 4812 (2000).
14. Hutter, R., Mallat, T., and Baiker, A., *J. Catal.* **157**, 665 (1995).
15. Thomas, J. M., Sankar, G., Klunduk, M. C., Attfield, M. P., Maschmeyer, T., Johnson, B. F. G., and Bell, R. G., *J. Phys. Chem. B* **103**, 8809 (1999).
16. Kataoka, T., and Dumesic, J. A., *J. Catal.* **112**, 66 (1988).
17. Liu, Z., Tabora, J., and Davis, R. J., *J. Catal.* **149**, 117 (1994).
18. Miller, J. B., Johnston, S. T., and Ko, E. I., *J. Catal.* **150**, 311 (1994).
19. Notari, B., *Adv. Catal.* **41**, 253 (1996).
20. Khouw, C. B., Dartt, C. B., Labinger, J. A., and Davis, M. E., *J. Catal.* **149**, 195 (1994).
21. Hutter, R., Mallat, T., Peterhans, A., and Baiker, A., *J. Mol. Catal. A* **138**, 241 (1999).
22. Sheldon, R. A., and Doorn, J. A. V., *J. Catal.* **31**, 427 (1973).
23. Dusi, M., Beck, C., Mallat, T., and Baiker, A., *in* "Catalysis of Organic Reactions" (M. E. Ford, Ed.), p. 315. Dekker, Allentown, PA, 2000.

24. Beck, C., Mallat, T., and Baiker, A., *Catal. Lett.* **75**, 131 (2001).
25. Corma, A., Domine, M., Gaona, J. A., Jorda, J. L., Navarro, M. T., Rey, F., Perez-Pariente, J., Tsuji, J., McCulloch, B., and Nemeth, L. T., *Chem. Commun.* 2211 (1998).
26. Deng, Y., and Maier, W. F., *J. Catal.* **199**, 115 (2001).
27. Dusi, M., Mallat, T., and Baiker, A., *J. Catal.* **187**, 191 (1999).
28. Müller, C. A., Maciejewski, M., Mallat, T., and Baiker, A., *J. Catal.* **184**, 280 (1999).
29. Kochkar, H., and Figueras, F., *J. Catal.* **171**, 420 (1997).
30. Dutoit, D. C. M., Schneider, M., and Baiker, A., *J. Por. Mat.* **1**, 165 (1995).
31. Bu, J., and Rhee, H. K., *Catal. Lett.* **65**, 141 (2000).
32. Martens, J. A., Buskens, P., Jakobs, P. A., Pol, A. v. d., Hooff, J. H. C. v., Ferrini, C., Kouwenhoven, H. W., Kooyman, P. J., and Bekkum, H. v., *Appl. Catal. A* **99**, 71 (1993).
33. Weber, R. S., *J. Catal.* **151**, 470 (1995).
34. Tatsumi, T., Koyano, K. A., and Igarashi, N., *J. Chem. Soc., Chem. Commun.* 325 (1998).
35. D'Amore, M. B., and Schwarz, S., *Chem. Commun.* 121 (1999).
36. Wulff, H. P., US Patent 3,923,843, 1975.
37. Gao, X., and Wachs, I. E., *Catal. Today* **51**, 233 (1999).
38. Fernandez, A., Leyrer, J., Gonzalez-Elipe, A. R., Munuera, G., and Knözinger, H., *J. Catal.* **112**, 489 (1988).
39. Lassaletta, G., Fernandez, A., Espinos, J. P., and Gonzalez-Elipe, A. R., *J. Phys. Chem.* **99**, 1484 (1995).
40. Jorgensen, C. K., "Modern Aspects of Ligand Field Theory." North-Holland, Amsterdam, 1971.
41. Boccuti, M. R., Rao, K. M., Zecchina, A., Leofanti, G., and Petrini, G., *Stud. Surf. Sci. Catal.* **48**, 133 (1989).
42. Klein, S., Weckhuysen, B. M., Martens, J. A., Maier, W. F., and Jacobs, P. A., *J. Catal.* **163**, 489 (1996).
43. Zechina, A., Spoto, G., Bordiga, S., Ferrero, A., Petrini, G., Padovan, M., and Leofanti, M., *Stud. Surf. Sci. Catal.* **69**, 251 (1991).
44. Lamberti, C., Bordiga, S., Zecchina, A., Carati, A., Fitch, A. N., Artioli, G., Petrini, G., Salvalaggio, M., and Marra, G. L., *J. Catal.* **183**, 222 (1999).
45. Mantegazza, M. A., Petrini, G., Spano, G., Bagatin, R., and Rivetti, F., *J. Mol. Catal. A* **146**, 223 (1999).
46. Orcel, G., Phalippou, J., and Hench, L. L., *J. Non-Cryst. Solids* **88**, 114 (1986).
47. Odenbrand, C. U. I., Andersson, S. L. T., Andersson, L. A. H., Brandin, J. G. M., and Busca, G. J., *J. Catal.* **125**, 541 (1990).
48. Uguina, M. A., Ovejero, G., Grieken, R. V., Serrano, D. P., and Camacho, M., *J. Chem. Soc. Chem. Commun.* 27 (1994).
49. Dutoit, D. C. M., Schneider, M., and Baiker, A., *J. Catal.* **153**, 165 (1995).
50. Schraml-Marth, M., Walther, K. L., Wokaun, A., Handy, B. E., and Baiker, A., *J. Non-Cryst. Solids* **143**, 93 (1992).
51. Vansant, E. F., VanDerVoort, P., and Vrancken, K. C., *Stud. Surf. Sci. Catal.* **93**, 3 (1995).
52. Sohn, J. R., and Hang, H. J., *J. Catal.* **132**, 563 (1991).
53. Miller, J. B., Mathers, L. J., and Ko, E. I., *J. Mater. Chem.* **5**, 1759 (1995).
54. Duran, A., Serna, C., Fornes, V., and Fernandez-Navarro, J. M., *J. Non-Cryst. Solids* **82**, 69 (1986).
55. Gao, X., Bare, S. R., Fierro, J. L. G., Banares, M. A., and Wachs, I. E., *J. Phys. Chem. B* **102**, 5653 (1998).
56. Stakheev, A. Y., Shpiro, E. S., and Apijok, J., *J. Phys. Chem.* **97**, 202 (1993).
57. Galan-Fereres, M., Alemany, L. J., Mariscal, R., Banares, M. A., Anderson, J. A., and Fierro, J. L. G., *Chem. Mater.* **7**, 1342 (1995).
58. Dusi, M., Mallat, T., and Baiker, A., *J. Mol. Catal. A* **138**, 15 (1999).
59. Arends, I., Seldon, R. A., Wallau, M., and Schuchardt, U., *Angew. Chem.* **36**, 1144 (1997).
60. Notari, B., *Stud. Surf. Sci. Catal.* **37**, 413 (1988).
61. Bellussi, G., and Rigutto, M. S., *Stud. Surf. Sci. Catal.* **85**, 177 (1994).
62. Klunduk, M. C., Maschmeyer, T., Thomas, J. M., and Johnson, B. F. G., *Chem. Eur. J.* **5**, 1481 (1999).
63. Karlsen, E., and Schöffel, K., *Catal. Today* **32**, 107 (1996).
64. Sinclair, P. E., and Catlow, C. R. A., *J. Phys. Chem. B* **103**, 1084 (1999).
65. Doolin, P. K., Alerasool, S., Zalewski, D. J., and Hoffman, J. F., *Catal. Lett.* **25**, 209 (1994).
66. Nishiwaki, K., Kakuta, N., Ueno, A., and Nakabayashi, H., *J. Catal.* **118**, 498 (1989).
67. Kosuge, K., and Singh, P. S., *J. Phys. Chem. B* **103**, 3563 (1999).
68. Maschmeyer, T., Klunduk, M. C., Martin, C. M., Shephard, D. S., Thomas, J. M., and Johnson, B. F. G., *Chem. Commun.* 1847 (1997).
69. Bouh, A. O., Rice, G. L., and Scott, S. L., *J. Am. Chem. Soc.* **121**, 7201 (1999).
70. Müller, C. A., Schneider, M. S., Mallat, T., and Baiker, A., *J. Catal.* **192**, 448 (2000).
71. Seiyama, T., "Metal Oxides and Their Catalytic Actions." Kodansha, Tokyo, 1978.
72. Ricchiardi, G., de Man, A., and Sauer, J., *Phys. Chem. Chem. Phys.* **2**, 2195 (2000).